CRUSHED DOLERITE ROCK PARTICLE SHAPE CHARACTERIZATION

Jaap Hoffmann[1] and Jeroen Houtappels[2]

[1] Dept. Mechanical & Mechatronic Engineering, Stellenbosch University, Private Bag X1, Matieland, 7602, South Africa; Phone: +27 808 3554; Fax: ; E-mail: hoffmaj@sun.ac.za

[2] Dept. of Mechanical Engineering, Eindhoven University of Technology; E-mail: j.g.f.houtappels@student.tue.nl

Abstract: Particle size and shape has a significant influence on the pressure drop and heat transfer characteristics of packed beds used as thermal energy storage for solar thermal power stations. The design and thermal capacity of rock beds depend on reliable predictions of the fluid flow paths and temperature profiles in the bed. Particle shape characterization is key in predicting flow paths and temperature profiles in the bed. The work reported here concerns the characterization of crushed rock particles, using 2D protocols. Results from the 2D protocols were validated against 3D scans of a subset of particles. Earlier work suggested that mon-dispersed ellipsoidal particles under-predict pressure drop and particles were separated into three different classes depending on their size and shape. Classifying particles into a few distinct shapes allows one to extract information on the packing structure and particle orientation from a discrete element model, whilst heat transfer and pressure drop information for a packed bed can be gleaned from computational fluid dynamics modelling of the flow in the interstitial volumes.

Keywords: Thermal energy storage, crushed rock, particle characterization

1. Introduction

Rapid depletion of fossil fuel resources and greenhouse gas emissions from their combustion spurred a drive towards renewable energy in the last two decades. Of the competing renewable energy sources, wind, hydro, solar photovoltaic (PV) and solar thermal are commercially deployed on large scale. In arid regions, there is limited potential for hydro energy, whilst wind- and solar PV energy require massive battery storage to become fully dispatchable. There is a massive drive worldwide to develop cheap battery storage on a utility-scale (IRENA, 2017) with limited commercial success thus far.

Solar thermal already benefits from large thermal energy storage (Labordena and Liliestam, 2015), but is more expensive than its competitors. Efforts to drive the cost of solar thermal energy down, focus on the inherent high thermal efficiency associated with central receiver systems, and reducing component costs (Boretti, 2018). One way of driving cost down is to use rock bed thermal energy storage, rather than molten salt. Allen (2014) estimated that the cost of rock bed storage should be about an order of magnitude lower than that of a molten salt thermal energy storage system.

Heller et al (2017) proposed a combined cycle, comprising of a solarized Brayton cycle, to be operated during the day, coupled asynchronously to a Rankine cycle that operates during the night or periods of extensive cloud cover. A rock bed energy storage system serves to store heat rejected by the Brayton cycle for later use. Using waste heat from the Brayton cycle not only increase the overall thermal efficiency of the plant but also enable it to deliver electricity on demand. Heller et al (2017) advocated the use of a dual pressure air receiver to overcome the limitations of a single receiver. The high-pressure side of the receiver feeds the gas turbine, whilst the low-pressure side dumps excess solar energy directly into the rock bed. A concept of a rock bed thermal energy storage system for utility-scale applications (Allen, 2014) is shown in figure 1. One can deduct from the figure that the flow through the rock bed will be fully three dimensional.

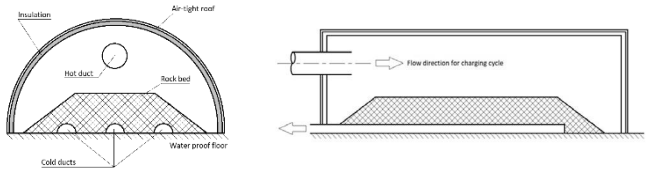

Figure 1. Concept of large rock bed thermal energy store.

Rock bed energy storage is still in the experimental phase, and test facilities (Okello et al, 2016; Klein, 2016; Allen, 2014) usually comprise small, prismatic beds subject to near plug flow conditions. Most researchers present their results in terms of packing density and spherical particles. The particle diameter is usually the volume equivalent diameter of the rocks. This is

understandable, as the bulk of the work in this field followed the lead of Ergun and Orning (1949), with a significant focus on wall channelling in later years (Achenbach, 1995; Hunt and Tien, 1990; Van Antwerpen et al, 2010), to name but a few. Laubscher et al (2017) considered flow through a conical rock pile. Although one would expect significant radial flow in this configuration, they did not attempt to isolate the contribution to pressure drop due to the radial and axial components of the flow. Efforts to compensate for the higher pressure drop through packed beds of irregular particles usually account for particle drag coefficient via a shape factor, of which sphericity is the most common (Singh et al, 2010). These results are not applicable where there is a significant deviation from plug flow conditions.

Following dimensional analysis, Hoffmann and Lindque (2019) argue that the pressure drop tensor for a packed bed of crushed rock particles should be given by

$$S_i = -\left\{\sum_{j=1}^{3} D_{ij}\mu v_j + \sum_{j=1}^{3} C_{ij}\tfrac{1}{2}\rho\left|\vec{V}\right|v_j\right\} \quad (1)$$

Where the coefficients D_{ij} and C_{ij} should depend on a characteristic length, say volume equivalent diameter, D_{ve}, sphericity, particle aspect ratio (taken as the ratio between the minimum and maximum cross-sectional area of the representative ellipsoid), surface roughness, ξ, overall bed length L_b and diameter D_b, the void fraction (porosity) ε and packing structure β, as well as the flow alignment with the particles, θ. The latter may be replaced by Herman's orientation factor (Li et al, 2019) in packed beds. The best fit to experimental results was found for the alignment angle being the angle between the short axis of the ellipsoid, L_S, and the mean flow direction. As aspect ratio and sphericity are both dimensionless, sphericity is interpreted as dependent on aspect ratio, and Hoffmann and Lindeque (2019) omitted sphericity from their final correlation. They also noted that an unambiguous description for packing structure does not seem to exist.

$$C_{ij} = f\left\{\left(\frac{\rho\bar{u}D_{ve}}{\mu}\right), \left(\frac{\xi}{D_{ve}}\right), \left(\frac{D_{ve}}{D_b}\right), \left(\frac{D_{ve}}{L_b}\right), \left(\frac{L_S}{L_L}\right), \varepsilon, \beta, \theta\right\} \quad (2)$$

Allen (2014), confirmed that the flow resistance in the pour direction of the crushed rock particles differs from that in the other directions, and concluded that it can be attributed to the way irregular particles pack down. To overcome the plug flow limit, Di Felice (1994) suggested that pressure drop should be correlated in terms of packing density and the drag coefficient of the particles in a free stream. Hölzer and Sommerfeld (2008) offer a simple correlation for the drag coefficient of irregular particles that depend on particle orientation. This approach is well suited for a representative unit cell formulation of packed beds (Du Plessis and Woudberg, 2008). With the advance in computational power, pore-scale modelling of packed beds has become feasible (Gan, 2015; Jafari, 2008; Li, 2019; Linsong, 2018), and the challenge has shifted to the proper characterization of irregular particles. Prescribing an ellipsoidal shape (Gan, 2015; Li et al, 2019; Taylor, 2006) to crushed rock particles have met with some success in capturing anisotropy in the flow field, but tend to under-predict the pressure drop (Hoffmann and Lindeque, 2019; Li et al, 2019).

Particle shape classification is an important topic, but it seems no consensus on the best shape descriptors has been reached. Galindo-Torrez et al (2012) state that the tortuosity tensor is a complex function of particle morphology, and implore researchers to pay attention to it. They introduced anisotropy into their packing by varying particle aspect ratio. Du et al (2016) found a strong correlation between particle sphericity and void size distribution that by implication should influence pressure drop through a packed bed. Li et al (2019) pointed out that particle orientation has a "profound effect" on pressure drop, something that sphericity on its own can't capture. Radoicic et al (2014) observed that small particles in a quartz sand sample (0.8 mm < D_{ve} < 1.25 mm) has higher sphericities (~ 0.85) than large particles (~ 0.7). They manually sorted particles into two groups, as shown in figure 6 in their paper. Coetzee and Nel (2014) proposed four groups, namely equant (cubic) particles (L ≈ I ≈ S), elongated particles (L » I ≈ S), flattened particles (L ≈ I » S) and intermediate particles that do not fit any of the other groups. L, I and S are the long, intermediate and short axes of the particle. L, I and S are orthogonal to each other. In a later paper, Coetzee (2016) proposed spherical (21 % of the sample), elongated (42 % of the sample) and tetrahedral (37 % of the sample) particles, based on laser scans of about 300 crushed rock particles up to 40 mm in size. These choices were informed by the capabilities of the discrete element (DEM) code PFC^{3D}, where the shapes were formed by single spherical particles (spheres), a clump of two spheres joined to each other (elongated) and a clump of four spheres at the corners of the tetrahedron. Coetzee (2016) found that by using more spheres to capture the shape of irregular particles, his DEM model's accuracy in predicting the bulk density of a packed bed of crushed rock increases.

In this paper, two-dimensional methods for particle characterization suggested by Taylor (2006), Bagheri et al (2015) and Diogaurdi and Mele (2015), applied to crushed dolerite rock particles, is described. Particles are by representative ellipsoids, as this shape best capture the effect of its orientation relative to the flow through the bed, as suggested by Li et al (2019). Particle characterization is seen as a necessary precursor to successful modelling of packed beds, which will lead in turn to better bed design in solar thermal power applications

2. Methodology

Dolerite is imminently suited for rock bed thermal energy storage. Allen (2014) has shown that after 1 500 thermal cycles, where the temperature was changed at a rate of 2 °C/min between 350 °C and 530 °C, dolerite shows no physical deterioration, except for some discolouration. Dolerite deposits largely overlap the region with the best solar resource in South Africa.

The rock samples considered in this paper was randomly selected by hand from a 20-ton pile of crushed dolerite rock in a size range from 53 mm to 75 mm. The rock pile has been exposed for more than five years to the elements, and most dust was washed away by rain. Individual particles were hand-selected; operators strived to ensure a random selection. Operator A (Hoffmann and Lindeque, 2019) selected 120 particles (sample I) and operator B (current work), 254 (sample II). A subset of 18 particles from sample II was selected for 3D scans (sample III).

Particles from sample III were weighed, and their volume extracted from 3D scans. This was used to calculate particle density. We found that the density of the particles is 2 909 kg/m^3 with a standard deviation of 40 kg/m^3 (1.4 %). This is in good agreement with densities recorded by Sloane (1991) for Tasmanian dolerite (2 850 – 3 010 kg/m^3), but about 9 % higher than those reported by Allen (2014) (2 567 kg/m^3). A constant particle density of 2 909 kg/m^3 was adopted in this study.

For the first batch of rocks (sample I), the particle mass was measured to within 0.01 g using a digital scale. The minimum bounding box ($L_L \times L_I \times L_S$) was measured to within 0.1 mm using a Vernier calliper. The particle volume V was calculated from the mass and assumed a constant density of 2 657 kg/m^3 after Allen (2014). From the particle volume, the diameter of the volume equivalent sphere was calculated. After averaging, a representative ellipsoidal particle was defined such that

$$\frac{A}{B} = \frac{\bar{L}_L}{\bar{L}_I} \quad and \quad \frac{C}{B} = \frac{\bar{L}_S}{\bar{L}_I} \tag{3}$$

with A, B and C the long, intermediate and short axes of the ellipsoid respectively. The volume of the ellipsoid corresponds to the mean volume equivalent diameter of the particles through

$$\frac{\pi ABC}{6} = \frac{\pi}{6}\left(\frac{\bar{L}_L}{\bar{L}_I}\right)\left(\frac{\bar{L}_S}{\bar{L}_I}\right)B^3 = \bar{V} = \frac{\pi D_{ve}^3}{6} \tag{4}$$

These monodispersed representative ellipsoids were used in experimental work and CFD/DEM simulations by Hoffmann and Lindeque (2019). Although they found good agreement between the experiments and simulations, their pressure drop was about a factor of two lower than that measured by Allen (2014) for crushed rock.

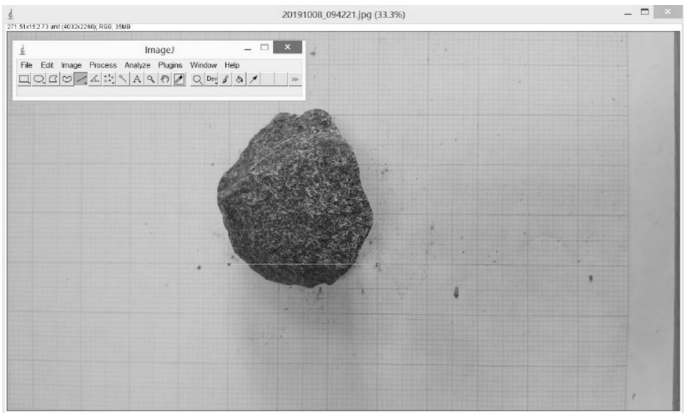

Figure 2. Calibrating the scale in Image-J.

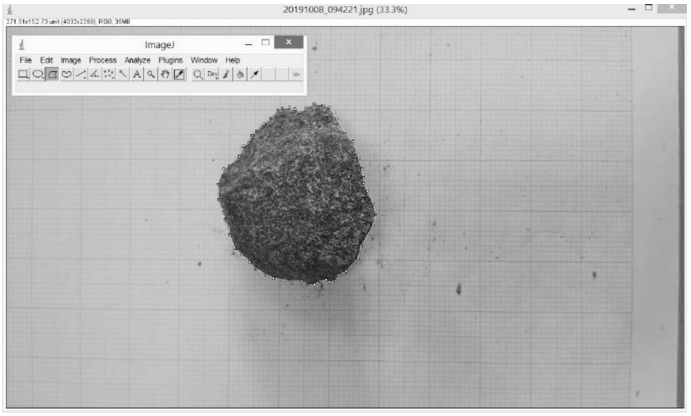

Figure 3. Capturing particle perimeter in Image-J.

For the second batch of rocks (sample II), the minimum bounding box and mass were measured as before. Following a suggestion by Bagheri et al (2015) that three orthogonal projections offer a good compromise between accuracy and processing time, measurements were expanded by taking images in three orthogonal planes of the particles. These images were processed, using the freeware product Image-J. For each image, the scale has to be set, using graph paper (figure 2). Image-J could not capture the particles automatically, and the outline of the particle had to be captured (figure 3) by hand. Capturing and processing three orthogonal images of a particle took between 5 and 10 minutes. Image-J outputs the projected area A, perimeter P, minimum bounding box, aspect ratio and Cox circularity of the projected particle. The latter is defined by

$$\phi = \frac{4\pi A}{P^2} \tag{5}$$

Rather than ϕ, we used $\bar{\phi}$ for which A and P is averaged over all three projections of the same particle. Bagheri et al (2015) also suggested that circularity $\bar{\phi}$ (a 2D shape descriptor) is a good estimate of sphericity ψ (a 3D shape descriptor), and thus one can estimate the surface area, SA, of the particle from the definition of sphericity

$$SA = \frac{\psi}{\pi D_{ve}^2} \quad (6)$$

with D_{ve} the diameter of the volume equivalent sphere. The latter is derived from the particle mass, assuming a constant density of 2 909 kg/m^3, as determined from sample III.

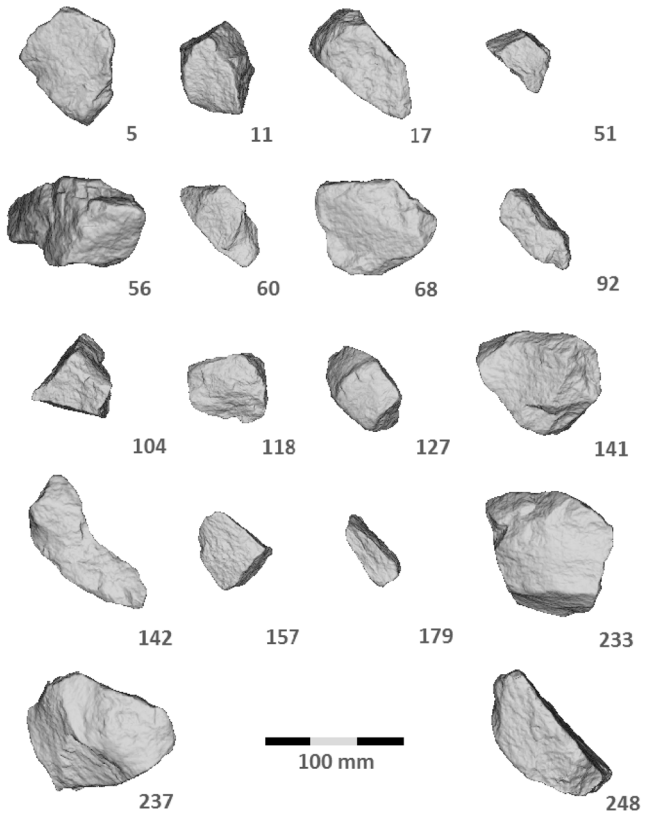

Figure 4. CAD rendering of particle shapes captured by 3D scanning.

The 2D projections were validated against 3D scans of a subset of 18 particles from sample B, as shown in figure 4. Particles were scanned, using an HP 3D Structured Light Scanner S3 Pro, with a resolution of 0.05 mm. Full 30° scanned profiles were exported to CAD software, where the surface area and volume of the scanned particles were extracted. The error in volume between the 3D scans (reference) and weight-based measurements ranged from -3.8 % and +2.5 % (average -0.01 %), whilst the error in surface area ranged from -14.0 % to +9.1 % (average -3.2 %). Errors in sphericity ranged from -16.0 % to +7.5 %, with an average error of -3.7 %. A plot of the sphericity measured in the 3D scans versus the 2D projections is given in figure 5. The dashed line represents the best linear fit on the data. The dashed line is forced through the origin of the graph. Our results support Bagheri et al's (2015) observation that projected area based protocols based upon three orthogonal projection give results with an accuracy of ± 10 %.

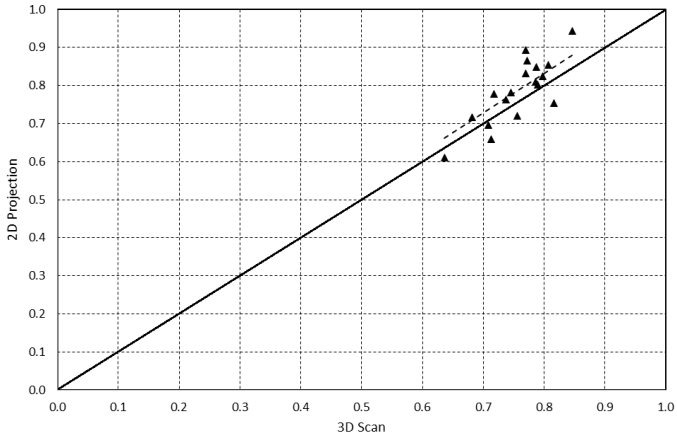

Figure 5. Comparison of particle sphericity measure by 2D projections versus 3D scans

3. Results and Discussion

There is good agreement between the three samples as far as elongation, here defined as L_L/L_I (i.e. the inverse of Bagheri et al's definition) and flatness are concerned, as shown in table 1. A larger difference (12 %) in particle equivalent diameter (in mm) was observed, which is partly explained by the different densities used, and partly by operator-related errors that may be as high as 5 % according to Bagheri et al (2015). The difference persisted even after the density of sample I was adjusted [sample I(a)]. Further interrogation of the data revealed that sample I contains a significantly higher percentage (75 %) of particles with L_L > 75 mm (upper sieve size) than sample II (56 %). One explanation is that during the two-year interval that elapsed between the two samplings, about 1.5 m^3 of rocks were frequently added to or removed from the rock pile for other tests. Samples were taken from the top of the pile.

Figure 6 shows that for particles in samples II and III, there is some correlation between aspect ratio and sphericity, as one would expect, but no discernible groupings. Sphericity range from about 0.6 to 0.9, with an average of 0.779. This is significantly higher than the values reported by Okonta and Magagula (2015) (0.67, with a standard deviation of 0. 094) from 3D scans of crushed rock samples from a dolerite quarry in Newcastle, South Africa. However, Okonta and Magagula measured only 10 particles, and their statistics are not expected to be representative of that the product from the quarry. Furthermore, their sample was meant for railway ballast, and contain a considerable amount of fines. As shown in figure 7, there is little correlation between particle size, as expressed by the diameter of its volume equivalent sphere, and sphericity. Sphericity for sample I was not calculated as the surface area was not measured.

Table 1. The mean particle aspect ratio for all samples

	Sample I	Sample I(a)	Sample II	Sample III	Sample I & II
(L_L/L_I)	1.505	1.479	1.480	1.465	1.488
(L_S/L_I)	0.641	0.630	0.639	0.616	0.640
D_e	59.5	57.7	51.0	53.0	51.3

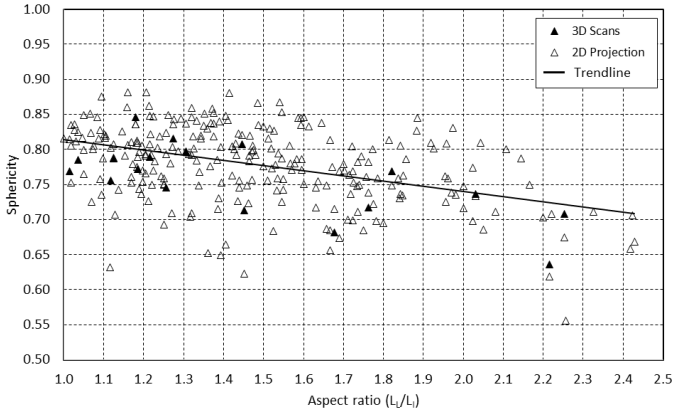

Figure 6. A plot of particle sphericity versus elongation.

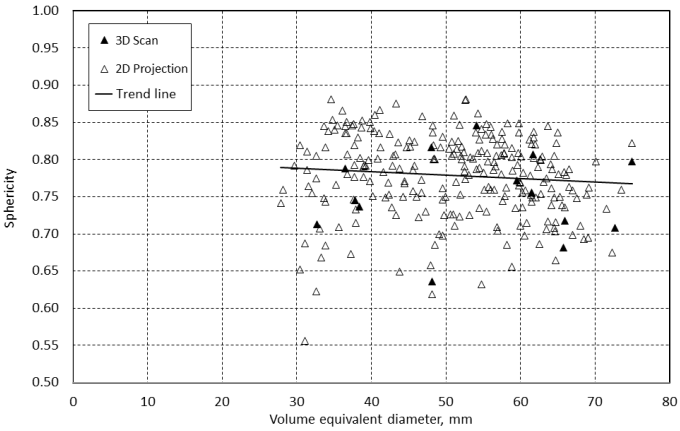

Figure 7. A plot of particle sphericity versus volume equivalent diameter.

We evaluated two different representative monodispersed shapes, namely an ellipsoid and a brick ($L \times W \times H$, with L the length, that corresponds to L_L, W the width that corresponds to L_I and H the height of the brick) to see how well they capture crushed rock particle characteristics captured in sample II. In both cases, the representative particle has the same volume, elongation and flatness as the crushed rock particles. The brick is defined such that

$$\frac{L}{W} = \frac{\bar{L}_L}{\bar{L}_I} \quad and \quad \frac{H}{W} = \frac{\bar{L}_S}{\bar{L}_I} \tag{7}$$

and

$$LWH = \left(\frac{\bar{L}_L}{\bar{L}_I}\right)\left(\frac{\bar{L}_S}{\bar{L}_I}\right) W^3 = \bar{V} \tag{8}$$

As seen from table 2, the bounding boxes of the ellipsoid and crushed rock particle are within 3 % of each other, whilst that of the brick is 21.7 % smaller than that of the crushed rock particle. The surface area of the representative ellipsoid is 8.4 % lower than that of the mean surface area of all the particles, and the surface area of the brick, 8.0 % higher. Due to its rounded shape, the sphericity of the ellipsoid is 14.5 % higher, and that of the brick 3.9 % lower than the mean sphericity of the crushed rock particles.

At face value, these numbers do not support one shape above the other. Discrete element modelling suggests that the ellipsoidal particles pack with a packing density of 34 %. Hoffmann and Lindeque (2019) reported an experimental value of 44 % for the packing factor for the ellipsoidal particles, whilst Allen (2014) reported a packing factor ranging between 41 and 47 % for crushed rock particles. By contrast, the packing factor for bricks, derived from discrete element modelling is 67 %.

Following the idea of Di Felice (1994), the drag force F_D on a particle in a packed bed is given by

$$F_D = f(\varepsilon) F_{D0} \tag{9}$$

F_{D0} is the drag force on the particle in a free stream, and $f(\varepsilon)$ a function of the particle superficial Reynolds number only. According to this formulation, the pressure drop across the more densely packed bed of ellipsoids will be 2.5 – 3.5 times higher than that across the less densely packed bed of bricks, despite the bricks having a much larger drag coefficient than the ellipsoids. Hoffmann and Lindeque (2019) found that the packed bed of ellipsoids under predicts the pressure drop across a packed bed of crushed rock. Thus, we conclude that bricks are not an appropriate approximation of rock shape when considering the pressure drop across rock beds.

The surface area of the ellipsoid used in this study is given by a simplified Knud Thomsen formula (Michon, 2020)

$$SA \approx 4\pi \left[\frac{(AB/4)^{8/5} + (AC/4)^{8/5} + (BC/4)^{8/5}}{3}\right]^{5/8} \tag{10}$$

with A, B and C the long, intermediate and short axes of the ellipsoid respectively. The accuracy of the equation above is within 1.5 %.

Particles from sample I and II combined were split into three groups, and their characteristics are listed in table 3. Group 1 represents particles that have L_L > 75 mm, meaning that they could only pass through a sieve with 75 × 75 mm aperture with L_L more or less perpendicular to the plane of the sieve. Group 2 comprised particles that have L_L < 75 mm and L_I > 53 mm, meaning that they would always be retained on a sieve with a 53

× 53 mm aperture. Particles in group 3 have L_I < 53 mm, and could theoretically pass through the sieve with 53 × 53 mm aperture if their L_L was more or less perpendicular to the plane of the sieve, but were somehow retained on the sieve. Group 1 contains mostly large (where large refers to the diameter of their volume equivalent spheres), elongated particles, group 2 large compact particles, and group 3 small elongated particles. Flatness shows the least variation across all groups. We did not observe the increase in sphericity with decreasing particle size, reported by Radoicic et al (2014).

Table 2. Comparison of mean particle parameters of crushed rock particles and approximate shapes

	Crushed rock	Ellipsoid	Brick
L_L [mm]	80.5	78.1	63.0
L_I [mm]	55.2	53.6	43.2
L_S [mm]	34.0	33.0	26.6
SA [mm^2]	11 235	9 687	11 491
ψ	0.779	0.892	0.748

Table 3. Particle shape descriptors after classification into groups based on size and shape.

	Group 1	Group 2	Group 3	All
L_L / L_I	1.589	1.151	1.406	1.488
L_S / L_I	0.618	0.634	0.691	0.640
D_e	56.8	50.0	39.7	51.3
N	228	44	102	374
Sphericity*	0.763	0.814	0.794	0.779

* Sample II only

4. Conclusion

Samples of 53 mm × 75 mm crushed dolerite rock were analysed, and some particle characteristics dimensions were extracted using 2D protocols. A total of 120 particles were measured by Vernier calliper only and a further 274 by 2D image processing. 3D scans of a small subset of the particles were used as a validation exercise and confirmed that agreement between the 2D and 3D protocols is within 4 %. This difference is of the same magnitude as operator errors (5 %) reported by Bagheri et al (2015).

Contrary to Radoicic et al (2014), our results indicate only a weak correlation (R^2 = 0.019) between sphericity and volume equivalent diameter. A much stronger correlation (R^2 = 0.227) exists between sphericity and elongation, but the scatter in the data is still significant. Since sphericity also fails to capture any effects of particle orientation in a packed bed, we concluded that sphericity is not a good indicator of particle shape, for our intended application at least.

Following ideas from Li et al (2019) and Hoffmann and Lindeque (2019), we decided on ellipsoids as representative shapes for crushed dolerite rock particle shape. Given that mono-dispersed ellipsoidal particle under-predicts the pressure drop across a bed of crushed rock articles, this work is aimed towards poly-dispersed particles. We have separate particles into three classes: those that could only pass the 75 mm sieve with their long axes perpendicular to the sieve, those that could pass the 75 mm sieve in orientation but would always be retained on the 53 mm sieve, and those that could have passed through the 53 mm sieve given the right orientation, but were retained. Based on the number of particles per group, 61 % of particles ended up in the first group, 12 % in the second, and 27 % in the third group. The elongation of the second group differs significantly from the other two groups, whilst flatness remains almost the same across all groups. Particle equivalent volume decreases continuously from group 1 to 3.

Although brick-shaped particles could theoretically capture particle orientation in a packed bed, discrete element modelling results suggests that the packing density for bricks is much lower than that of ellipsoids. According to Di Felice (1994), the effect of packing density on the pressure drop across a packed bed is more significant than that of the drag coefficient of the particles themselves. As a result, we discarded bricks as representative shapes for crushed rock particles when the interest is on the pressure drop across the bed.

References

[1] IRENA (2017), Electricity Storage and Renewables: Costs and Markets to 2030, International Renewable Energy Agency, Abu Dhabi.

[2] M. Labordena and J. Lilliestam, Cost and transmission requirements for reliable solar electricity from deserts in China and the United States, Energy Procedia, 76 (2015) 77 – 86.

[3] A. Boretti, Cost and production of solar thermal and solar photovoltaic power plants in the United States, Renewable Energy Focus, 2 (2018) 93 – 99.

[4] Allen, K.G., (2014), Rock bed thermal storage for concentrating solar power plants, PhD Thesis, Stellenbosch University.

[5] L.J. Heller, K.G. Allen, M. Lubkoll, J.P. Pitot de la Beaujardiere, P. Gauche and J.E. Hoffmann, The SUNDISC cycle: a direct storage-charging dual-pressure air receiver cycle, Solar Energy, 153 (2017) 435 – 444.

[6] D. Okello, O.J. Nydal, K. Nyeinga and E.J.K. Banda, Experimental investigation of heat extraction from a rock bed heat storage system for high-temperature applications, Journal of Energy in Southern Africa, 27 (2016) 30 – 37.

[7] P. Klein, (2016), High temperature packed bed thermal storage for solar gas turbines, PhD Thesis, University of the Witwatersrand.

[8] S. Ergun and A.A. Orning, Fluid flow through randomly packed columns and fluidized beds, Industrial and Engineering Chemistry, 41 (1949) 1179 –1184.

[9] E. Achenbach, Heat and flow characteristics of packed beds, Experimental and Thermal Fluid Sciences, 10 (1995) 17 – 27.

[10] M.L. Hunt and C.L. Tien, Non-Darcian flow, heat and mass transfer in catalytic packed-bed reactors, Chemical Engineering Science, Vol. 45 (1990) 55 – 63.

[11] W. van Antwerpen, C.G. du Toit and P.G. Rousseau, A review of correlations to model the packing structure and effective thermal conductivity in packed beds of mon-sized spherical particles, Nuclear Engineering and Design, 240 (2010) 1803 – 1818.

[12] H.F. Laubscher, T.W. von Backström and F. Dinter, Developing a cost-effective rock bed thermal energy storage system: design and modelling, AIP Conference Proceedings, 1850 (2017) 080015.

[13] H. Singh, R.P. Saini and J.S. Saini, A review on packed bed solar energy storage systems, Renewable and Sustainable Energy Reviews, 14 (2010) 1059 – 1069.

[14] J.E. Hoffmann and P.J. Lindeque, (2019), Pressure Drop Through Randomly Packed Beds of Ellipsoidal Particles, Proceedings of HEFAT 2019, Wicklow.

[15] X. Li, M. Jiang, Z. Huang and Q. Zhou, Effect of particle orientation on the drag force in random arrays of prolate ellipsoids in low-Reynolds-number flows, AIChE Journal, 65 (2019) 1 – 11.

[16] R. Di Felice, The voidage function for fluid-particle interaction systems, International Journal of Multiphase Flow, 20 (1994) 153 – 159.

[17] A. Hölzer and M. Sommerfeld, New simple correlation formula for the drag coefficient of non-spherical particles, Powder Technology, 184 (2008) 361 – 365.

[18] J.P. du Plessis and S. Woudberg, Pore-scale derivation of the Ergun equation to enhance its adaptability and generalization, Chemical Engineering Sciences, 63 (2008) 2576 – 2586.

[19] J. Gan, Z. Zhou and A. Yu, Particle scale study of heat transfer in packed and fluidized beds of ellipsoidal particles, Chemical Engineering Science, 144 (2015) 201 – 215.

[20] A. Jafari, P. Zamankhan, S.M. Mousavi and K. Pietarinen, Modeling and CFD simulation of flow behaviour and dispersivity through randomly packed bed reactors, Chemical Engineering Journal, 144 (2008) 476 – 482.

[21] J. Linsong, L. Hongsheng, W. Dan, W. Jiansheng and X. Maohao, Pore-scale simulation of vortex characteristics in randomly packed beds using LES/RANS models, Chemical Engineering Science, 177 (2018) 431 – 444.

[22] M.A. Taylor, E.J. Garboczi, S.T. Erdogan and D.W. Fowler, Some properties of irregular 3-D particles, Powder Technology, 12 (2006) pp. 1 – 15.

[23] S.A. Galindo-Torrez, A. Scheuermann and L. Li, A numerical study on the permeability in a tensorial form for laminar flow in anisotropic porous media, Physical Review E, 86 (2012), 046306-1 – 046306-9.

[24] W. Du, N. Quan, P. Lu, J. Xu, W. Wei and L. Zhang, Experimental and statistical analysis of the void size distribution and pressure drop validations in packed beds, Chemical Engineering and Design, 106 (2016) 115 – 125.

[25] T.K. Radoicic, M. Duris, R. Garic-Grolovic, Z. Arsenijevic and Z. Grbavcic, Particle characterization of polydisperse quartz filtration sand, Powder Technology, 254 (2014), 63 – 71.

[26] C.J. Coetzee and R.G. Nel, Calibration of discrete element properties and the modelling of packed rock beds, Powder Technology, 264 (2014) 332 – 342.

[27] C.J. Coetzee, Calibration of the discrete element method and the effect of particle shape, Powder Technology, 29 (2016) 50 – 70.

[28] G.H. Bagheri, C. Bonadonna, I. Manzella and P. Vonlanten, On the characterization of size and shape of irregular particles, Powder Technology, 270 (2015) 141 – 153.

[29] F. Dioguardi and D. Mele, A new shape-dependent drag correlation formula for non-spherical rough particles: experiments and results, Powder Technology, 277 (2015) 222 – 230.

[30] D.J. Sloane, (1991), Some physical properties of dolerite, Tasmania Department of Resources and Energy, Division of Mines and Resources, Report 1991/22.

[31] F.N. Okonta and S.G. Magagula, Railway foundation properties of some South African quarry stones, Electronic Journal of Geotechnical Engineering, 16 (2008) 179 – 197.

[32] G.P. Michon, (2020), Spheroids and scalene ellipsoids, http://www.numericana.com/answer/ ellipsoid.htm#thomsen, accessed 17 July 2020.